

Article

Deep Learning-Based Classification of High-Resolution Satellite Images for Mangrove Mapping

Yidi Wei ¹, Yongcun Cheng ², Xiaobin Yin ¹, Qing Xu ^{1,*}, Jiangchen Ke ² and Xueding Li ^{3,*}

¹ College of Marine Technology, Faculty of Information Science and Engineering, Ocean University of China, Qingdao 266100, China; weiyidi@stu.ouc.edu.cn (Y.W.)

² PIESAT Information Technology Co., Ltd., Beijing 100195, China

³ Fujian Marine Forecasts, Fuzhou 350003, China

* Correspondence: xuqing@ouc.edu.cn (Q.X.); lxd007@xmu.edu.cn (X.L.)

Abstract: Detailed information about mangroves is crucial for ecological and environmental protection and sustainable development. It is difficult to capture small patches of mangroves from satellite images with relatively low to medium resolution. In this study, high-resolution (0.8–2 m) images from Chinese GaoFen (GF) and ZiYuan (ZY) series satellites were used to map the distribution of mangroves in coastal areas of Guangdong Province, China. A deep-learning network, U²-Net, with attention gates was applied to extract multi-scale information of mangroves from satellite images. The results showed that the attention U²-Net model performed well on mangrove classification. The overall accuracy, precision, and F1-score values were 96.5%, 92.0%, and 91.5%, respectively, which were higher than those obtained from other machine-learning methods such as Random Forest or U-Net. Based on the high-resolution mangrove maps generated from long satellite image time series, we also investigated the spatiotemporal evolution of the mangrove forest in Shuidong Bay. The results can provide crucial information for government administrators, scientists, and other stakeholders to monitor the dynamic changes in mangroves.

Keywords: mangrove classification; U²-Net; attention gate



Citation: Wei, Y.; Cheng, Y.; Yin, X.;

Xu, Q.; Ke, J.; Li, X. Deep

Learning-Based Classification of

High-Resolution Satellite Images for

Mangrove Mapping. *Appl. Sci.* **2023**,

13, 8526. [https://doi.org/10.3390/](https://doi.org/10.3390/app13148526)

[app13148526](https://doi.org/10.3390/app13148526)

Academic Editor: Antonio

Fernández-Caballero

Received: 19 June 2023

Revised: 13 July 2023

Accepted: 20 July 2023

Published: 24 July 2023



Copyright: © 2023 by the authors.

Licensee MDPI, Basel, Switzerland.

This article is an open access article

distributed under the terms and

conditions of the Creative Commons

Attribution (CC BY) license ([https://](https://creativecommons.org/licenses/by/4.0/)

[creativecommons.org/licenses/by/](https://creativecommons.org/licenses/by/4.0/)

[4.0/](https://creativecommons.org/licenses/by/4.0/)).

1. Introduction

Mangrove forests are one of the typical marine ecosystem landscapes, which are distributed in tropical and subtropical coastal areas. They are also known as the “green lung of the ocean”, as they provide various ecological and economic benefits, such as purifying seawater, storing carbon, maintaining biodiversity, and protecting the coastline from erosion and storms. In recent years, positive progress has been made in protecting and restoring mangroves around the world, as more people have recognized their value and importance. However, mangroves are still facing many threats, such as deforestation, urbanization, pollution, and climate change. These threats can lead to habitat degradation and biodiversity reduction, which can affect the functions and services of mangroves. Therefore, it is necessary to enhance the monitoring capabilities and produce more detailed maps of mangroves, which can help the management and protection of mangroves [1]. The maps can provide useful information for assessing the status and trends of mangroves and designing appropriate strategies for sustainable management of mangroves.

In China, mangroves are mainly distributed in Guangdong, Guangxi, Hainan, Fujian, and Zhejiang provinces, and they are mainly located in the tidal flat area [2]. Compared to other terrestrial ecosystems, field surveys in mangrove areas are more time-consuming and laborious [3]. Remote sensing is an ideal choice for quantitative monitoring of the distribution and extent of mangroves due to its advantages of wide coverage and high effectiveness [4]. However, mangrove monitoring capability is influenced by the extraction method and the resolution of satellite sensors [5]. At present, classification methods commonly used for mangrove mapping from satellite images mainly include pixel-based

and object-oriented classifications [6–10]. Kanniah et al. [6] used IKONOS image and corresponding texture information to classify mangroves based on pixel maximum likelihood classification (MLC), with an overall accuracy of 82%. Wang et al. [7] used Pleiades-1 satellite images and the Random Forest (RF) algorithm to classify mangroves in the Nansha wetland, and the overall accuracy was 82.4%. However, traditional pixel-based classification has a “pepper and salt” problem, which shows a discrete and random distribution of white or black pixels in an image. Object-oriented classification uses both spectral characteristics and texture information of mangroves, avoiding the “pepper and salt” problem. Pham et al. [8] used an object-based logistics model tree (LMT) algorithm to map the distribution of mangroves from 2010 to 2015 based on ALOS-2 PALSAR imagery, and they obtained an overall accuracy of 83.8%.

In recent years, deep learning methods have been widely applied to coastal and offshore environmental monitoring such as waterline extraction [11], flood mapping [12], sea subsurface temperature reconstruction [13], etc. With the development of deep learning in the field of image recognition, the application of deep learning in mangrove monitoring has also become a research hotspot. Iovan et al. [14] proposed a deep convolutional neural network (CNN) that automatically detects mangroves over Fiji in the South Pacific Ocean from Sentinel-2 and World-View 2 images with resolutions of 10 m and 50 m, respectively. Huang et al. [15] applied the LeNet-5 network to extract mangrove species information from unmanned aerial vehicle (UAV) images, resulting in an overall recognition rate of 87.31%. Guo et al. [16] achieved an overall accuracy of 87% when using a deep-learning model called Capsules-Unet for monitoring mangroves in Hainan Island from Landsat-5 TM (Thematic Mapper), Landsat-7 ETM+ (Enhanced Thematic Mapper Plus), and Landsat-8 OLI (Operational Land Imager and TIRS) images with a resolution of 30 m. Most of these studies focused on mangrove extraction based on relatively low- to medium-resolution satellite data, with resolution values up to 10 m. However, the number of small mangrove patches with an area of less than 1 hectare (ha) is increasing in China [17]. Therefore, it is necessary to obtain more detailed information about mangroves from higher-resolution satellite images.

In this study, we aim to provide high-resolution maps of mangroves in coastal areas of Guangdong Province, China. A deep learning network, U²-Net, combined with an attention gate was proposed to extract multi-scale features of mangroves from Chinese GF and ZY satellite images with a resolution of up to 0.8 m. The remainder of the paper is organized as follows: Section 2 describes the study area, satellite data sources, and the methodology. The performance of the attention U²-Net model is explained in Section 3. A case study on the spatiotemporal evolution of the mangrove forest in Maoming Shuidong Bay based on satellite observations is introduced in Section 4. The conclusion is given in Section 5.

2. Materials and Methods

2.1. Study Area

Guangdong Province is one of the areas with the widest mangrove distribution and the most complete diversity of mangrove species in China. According to the latest statistics, the total area of mangroves in Guangdong is currently about 14,000 ha, accounting for about 56.9% of the total mangrove area in China. We selected the coastal area of Maoming, Zhanjiang, and Taishan cities as the study area. Figure 1 shows the locations of Maoming, Taishan, and Zhanjiang in the southwest of Guangdong Province, China. These cities have a typical subtropical and monsoon-influenced climate characterized by hot, humid, and rainy summers and mild winters [18]. The annual temperature ranges from 22.6 °C to 24.2 °C, with January being the coolest month and July to August being the warmest months. Rainfall peaks from May to September, with August receiving the most precipitation. The dry and sunny season lasts from December to January. The cities are also exposed to tropical cyclones from June to November, which can cause strong winds, heavy rains, and storm surges.

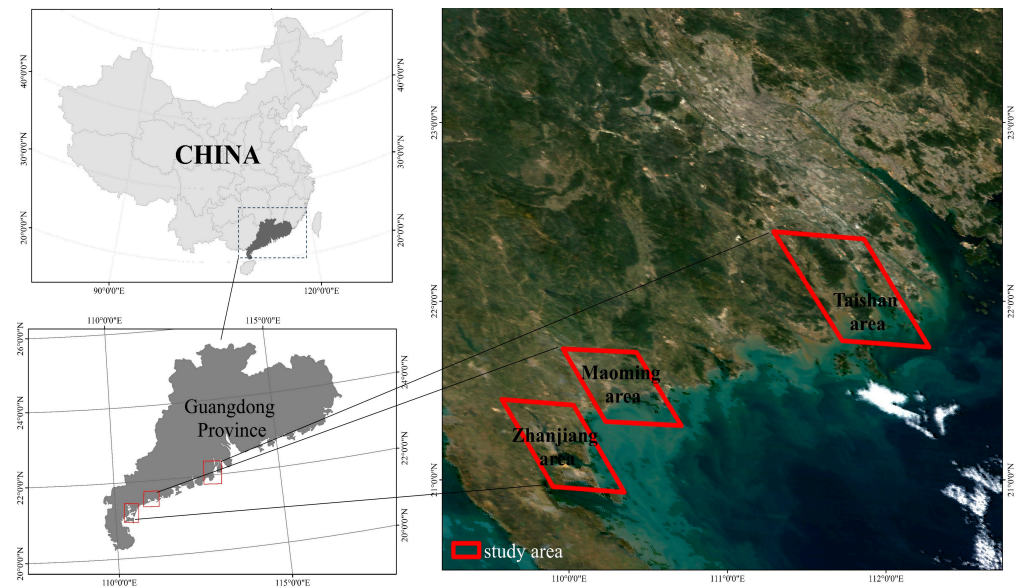


Figure 1. Study area.

2.2. Satellite Data

High-resolution remote sensing images used in this study were from Chinese GF-1, GF-2, GF-6, and ZY-3 satellites. There are currently four GF-1 series satellites operating in orbit. The first satellite, GF-1 01, was successfully launched on 26 April 2013. The PMS (panchromatic/multi-spectra) onboard GF-1 satellites provide panchromatic and multispectral images with resolutions of 2 m and 8 m, respectively. GF-2, which was launched on 19 August 2014, has a spatial resolution of 0.8 m in the panchromatic band and 3.24 m in the multi-spectral band. GF-6 is a low-orbit optical satellite. The onboard PMS provides images with the same resolution as GF-1. ZY-3 01 is the first autonomous high-resolution stereoscopic mapping satellite for civil use in China, launched on 9 January 2012, which provides panchromatic and multispectral images with resolutions of 2.1 m and 5.8 m, respectively.

In order to extract information of small mangrove patches, we used optical images with a resolution higher than 2 m in this study. In total, 35 scenes of images were collected with cloud coverage values of less than 10%. The information of these images is shown in Table 1. These images were processed by atmospheric correction, orthophoto correction, image fusion, and true color synthesis (Figure 2).

Table 1. Information of satellite images.

Satellite-Sensor	Date (MM/DD/YY)	Area	Spatial Resolution	Image Size
GF1-PMS1	09/20/2018	Maoming	Multi Spectral Scanner (MSS): 8 m Panchromatic (PAN): 2 m	36 km × 36 km
	05/16/2019			
	11/25/2019			
	10/20/2015			
	01/13/2018	Taishan		

Table 1. *Cont.*

Satellite-Sensor	Date (MM/DD/YY)	Area	Spatial Resolution	Image Size
GF1-PMS2	09/30/2014	Zhanjiang	MSS: 8 m PAN: 2 m	36 km × 36 km
	10/02/2014			
	03/20/2018	Maoming		
	06/03/2014			
	09/26/2014			
	06/07/2015			
	01/01/2017			
	10/26/2020			
01/25/2017	Taishan			
GF2-PMS1	03/22/2018	Maoming	MSS: 4 m PAN: 0.8 m	28 km × 28 km
	01/02/2018	Taishan		
	12/02/2016			
	12/08/2016			
GF2-PMS2	01/22/2017	Zhanjiang	MSS: 4 m PAN: 0.8 m	28 km × 28 km
	03/15/2020	Maoming		
	11/08/2019			
	11/30/2015	Taishan		
	07/21/2020			
GF6-PMS	02/21/2020	Zhanjiang	MSS: 8 m PAN: 2 m	96 km × 96 km
	12/01/2019	Taishan		
ZY3-TMS	03/02/2017	Zhanjiang	2.5 m	52 km × 52 km
	01/10/2015	Maoming		
	10/19/2017			
	10/24/2017			
	01/22/2017	Taishan		

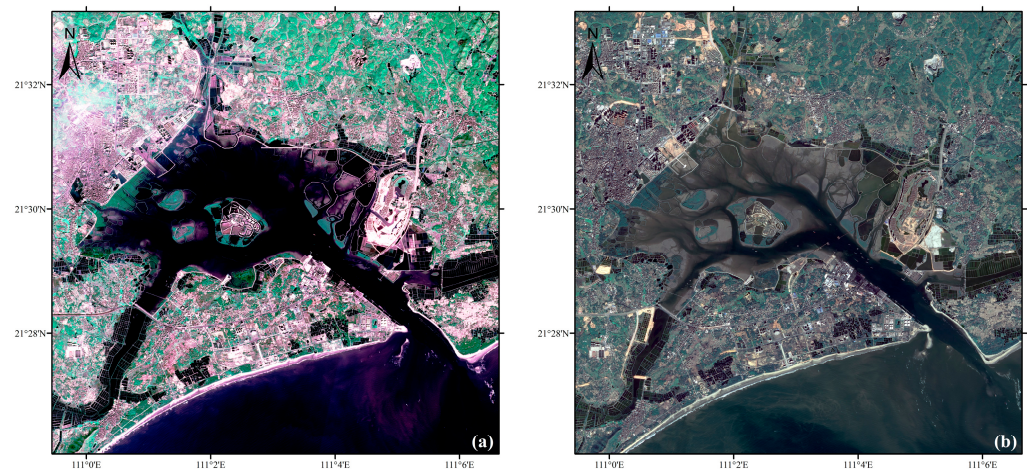


Figure 2. Examples of ZY-3 (a) and GF-6 (b) images in Maoming City.

PIE-Ortho 6.0 software [19] was used to preprocess the images. First, atmospheric correction was performed on the images using the fast line-of-sight atmospheric analysis of

spectral hypercubes (FLAASH) model [20]. These images were then orthorectified using reference images and DEM data (resolution of 30 m; <https://earthexplorer.usgs.gov/> (accessed on 25 October 2019)), and the Rational Polynomial Coefficients (RPC) model was applied for correcting the projection error and image geocoding. Next, the multispectral image and the panchromatic band image were registered using the orthorectified panchromatic band image as a reference to ensure that the registration accuracy between the two types of images did not exceed 0.5 pixels. The pansharpen algorithm [21] was used to fuse data, making the multispectral image highly similar to the original panchromatic band image and to reduce spectral distortion. Finally, a true color image was synthesized. These images were mosaicked by county-level administrative districts.

GF-2 images with a resolution of 0.8 m were all resampled to a grid size of 2 m. Since mangroves are mainly distributed in the coastal intertidal zone, the buffer zone was set to within 1 km of the coastline. Finally, all images were segmented into 2237 samples with a size of 320 × 320 pixels.

2.3. Attention U²-Net Model for Mangrove Detection

2.3.1. Structure of the Attention U²-Net

A combination of the deep learning model U²-Net and attention gate, hereafter called attention U²-Net, was adopted in this study for automatic mangrove detection from the high-resolution imagery. Attention U²-Net is based on U²-Net, which is a network for salient object detection proposed by Qin et al. [22]. As shown in Figure 3, the architecture of the network is a two-layer nested U structure. U²-Net consists of 6 coding layers, 5 decoding layers, and a full connection layer. Instead of a single convolution layer or deconvolution layer, each encoding and decoding layer embeds a complete Residual U-block (RSU) structure, which can extract multi-scale features during the sampling process. The RSU integrates the characteristics of the receptive field at different scales. This architecture allows researchers to train the deep network from scratch and improve the recognition efficiency by extracting multi-scale features layer by layer.

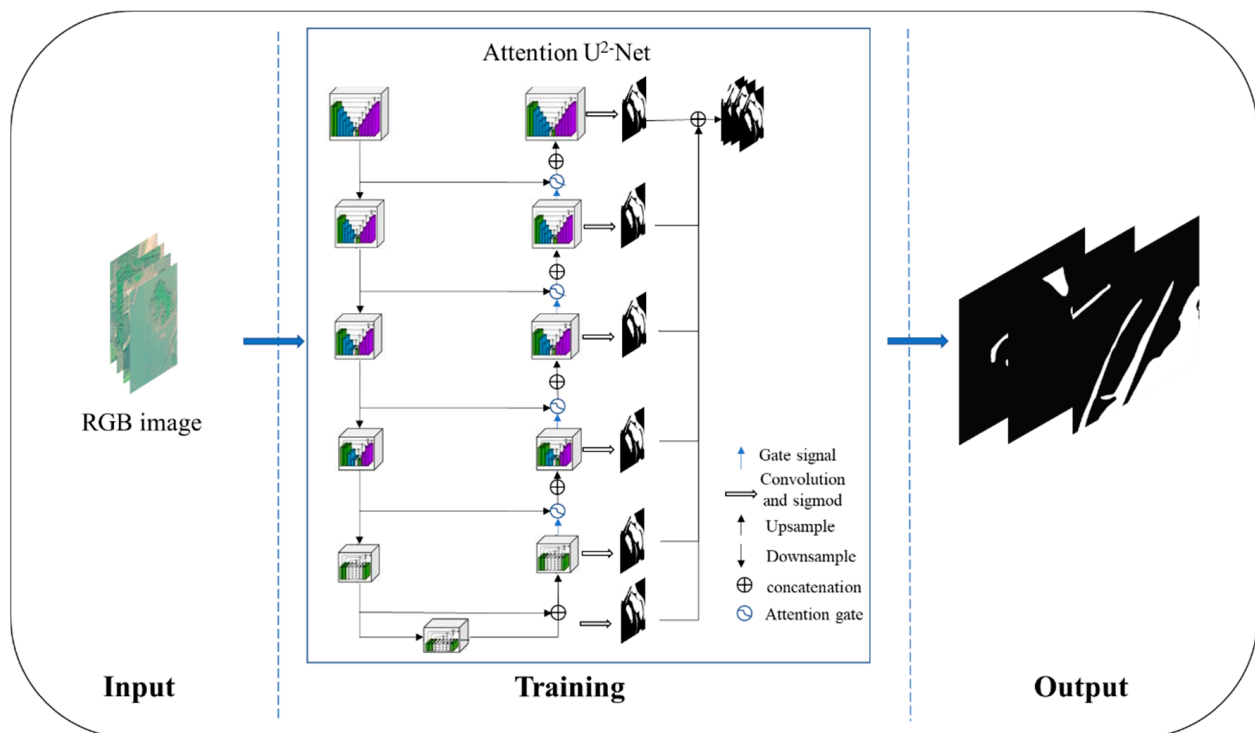


Figure 3. The structure of the attention U²-Net.

The mangrove training sample is a high-resolution satellite image that contains mangroves and other land cover types. The training sample is transmitted downward through resampling of the encoder, which reduces the spatial resolution but increases the feature dimension. The encoder can learn the low-level and high-level features of mangroves from the training sample. The resampled training sample is then transmitted to the decoder, which increases the spatial resolution but reduces the feature dimension. The decoder can reconstruct the mangrove map from the features learned by the encoder. The loss function is calculated at each level of the decoder, which measures the difference between the identified mangrove map and the ground truth map. The loss function is minimized through continuous iteration, which can update the network parameters and optimize the network performance. After traversing all the encoding layers and decoding layers, the feature extraction results are concentrated in the fully connected layer, which outputs the final mangrove extraction result. The final mangrove extraction result has the same size as the training sample, and it shows the location and shape of mangroves.

By embedding the attention gate into the U²-Net model, irrelevant regional features can be suppressed, and the model will pay more attention to the salient features of targets [23]. Figure 4 shows the structure of the attention gate. The attention gate consists of three parts: an input gate, an output gate, and an attention coefficient. The input gate receives the input features from the encoder and the decoder and performs a convolution operation on them. Firstly, one-dimensional convolution is performed on the input feature (x) downsampling from the top and gating signal (g) upsampling from the map below x . The purpose of convolution is to make the channel numbers of x and g consistent. Then, g and x are combined after the convolution operation, and the attention coefficient α [0, 1] is calculated through the ReLU function, one-dimensional convolution, and the sigmoid function on the input gate, which can assign different weights to different regions of the input features. The output gate performs another convolution operation on the input features and then multiplies them with the attention coefficient. Finally, the original x and α are multiplied to obtain the attention weight. The results of the attention gate are then concatenated with the upsampled results.

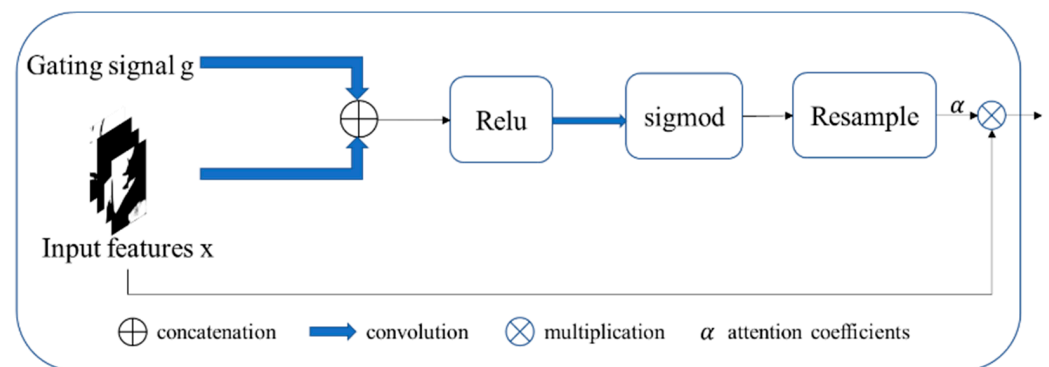


Figure 4. The structure of the attention gate: g is the gating signal, x is the input feature, and α is the attention coefficient.

2.3.2. Model Performance Evaluation Method

The performance of the attention U²-Net model is evaluated through the overall accuracy (OA), precision (P), and $F1$ -score ($F1$). The expression of these indices can be found in Formulas (3) to (5). OA is the percentage of all correct classifications in the total test data samples. P is the ability of the model to classify all positive classes. These metrics are commonly used to evaluate the quality of the model output, as they measure how well the model can correctly identify and classify the mangroves from the background. The

F1-Score is a metric that combines precision and recall, which are two indicators of how well the network can correctly identify and classify the mangroves from the background.

$$OA = \frac{(TP + TN)}{(TP + TN + FP + FN)} \quad (1)$$

$$P = \frac{TP}{TP + FP} \quad (2)$$

$$F1 = \frac{P \times R}{P + R} \quad (3)$$

where TP is the number of positive classes that are classified correctly, TN is the number of negative classes classified as negative, FP is the number of positive classes classified as negative, and FN is the number of negative classes classified as negative. R is recall, which can be expressed by

$$R = \frac{TP}{TP + FN} \quad (4)$$

For the binary classification task in this study, the confusion matrix could be represented as shown in Table 2. The confusion matrix is an analysis table that summarizes the prediction results of the classification model.

Table 2. Confusion matrix.

Confusion Matrix		Prediction	
		Positive (Mangrove)	Negative (Background)
Actual	Positive (Mangrove)	TP	FN
	Negative (Background)	FP	TN

2.3.3. Configuration of the Attention U²-Net

In order to train and test the attention U²-Net model for mangrove detection, we had to prepare a sample dataset from the satellite images. We used LabelMe 4.5 software, which is a tool for image annotation, to label the pixels in satellite images as either mangrove or non-mangrove (background). Similar to the method used in some studies on mangrove classification (e.g., [14]) 2020), labels were created through visual interpretation based on collected reference samples from high-resolution satellite imagery and previous mangrove maps. We removed the images that had less than 1% of mangrove pixels, as they are not suitable for mangrove detection. After this process, we obtained 2237 samples with a size of 320×320 pixels. The data volume was expanded to three times by further processing these images through horizontal flipping, vertical flipping, and random cropping. We split the dataset into two parts: 70% of the samples were used for model training, and the remaining 30% were used for model testing.

However, we encountered a problem of sample unbalancing in our dataset. The proportion of mangrove pixels to the total image pixels was only 19%, which means that most of the pixels belonged to the background rather than the mangrove target. This could cause the network to learn more features from the background and ignore the features from the mangrove target, which could affect the accuracy and reliability of mangrove detection. To solve this problem, we used a *loss* function that considers the contribution of F1-Score. By considering the F1-Score in the *loss* function, we could make the network learn more target features and balance the contribution of mangrove pixels and background pixels. The *loss* function is expressed as

$$loss = \alpha \times BCE + (1 - \alpha)(1 - F1) \quad (5)$$

where α is the factor that balances BCE and $F1$, and its value is set at 0.4. BCE is a traditional binary classification loss function that represents the difference between the measurement x_i and the classified value y_i .

$$BCE = -\sum_{i=1}^N [y_i \ln(\sigma(x_i)) + (1 - y_i) \ln(1 - \sigma(x_i))] \quad (6)$$

where N is the number of samples; y_i is the label of sample i , where y_i is 1 if the sample is mangrove and 0 if it is not; and $\sigma(x_i)$ represents the probability that sample i is classified as mangrove.

In addition, a series of comparative experiments was conducted to determine the optimal model parameter combination by adjusting the values of batch size (b_n), learning rate, and epoch number. We set b_n to 2, 8, 16, and 32; the learning rate to 0.0001, 0.001, and $0.1 \cdot b_n / 256$ [24]; and the number of epochs to 500, 1000, 1500, and 2000.

3. Results: Performance of the Attention U²-Net Model

Figure 5 shows the overall performance of the attention U²-Net model in mangrove classification based on the test dataset. We also carried out comparative experiments to compare our model with other machine-learning methods, including RF and U-Net. Examples of mangrove extraction results from four models are shown in Figure 6.

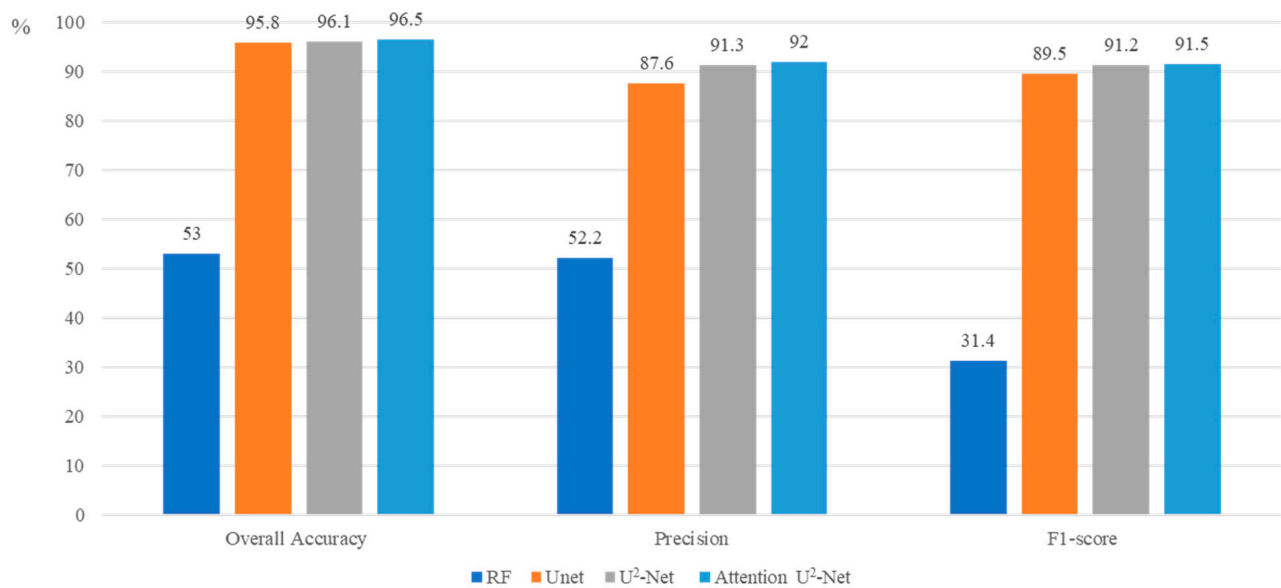


Figure 5. Mangrove classification results obtained from four models.

The results showed that the attention U²-Net model had the best performance among the four models, as it achieved the highest overall accuracy, precision, and F1-score. The values of overall accuracy, precision, and F1-score for the attention U²-Net model were 96.5%, 92.0%, and 91.5%, respectively, which were much higher than those obtained from the RF model, which had the lowest performance. The RF model tended to misclassify the spatial patterns that appeared smooth and uniformly colored on remote sensing images, such as water or bare land, as mangroves. Therefore, it exhibited a low precision of 52.2% and also a low overall accuracy and F1-score. Compared with the RF and U-Net models, the attention U²-Net model could almost completely extract mangroves from satellite images, as it has a deep learning architecture that could capture more features and details of mangroves. The U²-Net model had a high precision of 91.3%, which was significantly increased compared to the U-Net model. The U-Net model may have overestimated the area of mangroves, as it may have classified some small patches of mangroves as a few large patches, resulting in a coarse and inaccurate output (Figure 6d). After considering

the attention gate, although the overall performance of the attention U^2 -Net model was only slightly improved, more detailed information about mangroves could be extracted from this model (Figure 6f). The attention gate could help the model focus on the regions of interest and ignore the irrelevant regions, thus enhancing the quality of the output. The attention U^2 -Net model could extract more detailed information about mangroves from satellite images, such as their boundaries and shapes (Figure 6f). This indicates that our model performed quite well in effectively and accurately mapping mangroves and can provide useful information for mangrove conservation and management.

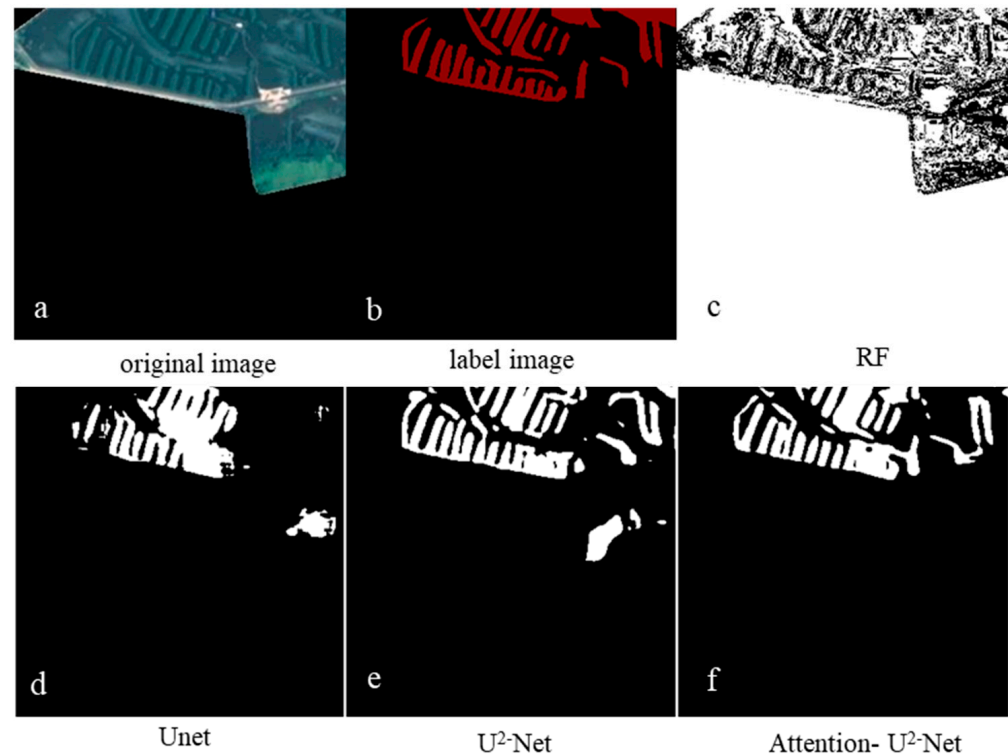


Figure 6. GF-1 image with 2 m resolution (a), mangrove label image (b), and classification results from four models: (c) RF, (d) U-Net, (e) U^2 -Net, and (f) attention U^2 -Net.

4. Discussion

4.1. Advantages and Limitations of the Attention U^2 -Net Model

In this study, we proposed and applied an attention U^2 -Net model for mangrove extraction from high-resolution satellite images. The results indicate that our model performs well in mangrove classification. The precision is 92.0%, which is much higher than that of the RF model (52.2%). As shown in Table 3, the attention U^2 -Net model may outperform some other machine-learning or deep-learning methods [25–28]. One possible reason is that the U^2 -Net can learn from data and optimize the algorithm and parameters automatically, without relying on manual feature extraction or selection. In addition, the attention U^2 -Net model can improve the accuracy and efficiency of mangrove mapping by using a complex and nonlinear network that can capture the spectral and spatial features of mangroves. The attention gate allows the model to focus on the most relevant regions and pixels for mangrove classification. The use of high-resolution images may also contribute to the improvement of model performance.

Table 3. Comparison of the performance of our model and other methods in mangrove classification.

Literature	Study Area	Satellite/Spatial Resolution	Method	Precision
Iovan et al. [14]	South Pacific Ocean	WorldView 2/0.5 m and Sentinel-2/20 m	A small-patched convolutional neural network	Detection rates are 87.94% with a false positive rate of 1.00%
Wang et al. [25]	Caribbean coast of Panama	Ikonos/0.58 m	Back propagation neural network (BPNN)	88.8%
			Clustering-based neural network classifier (CBNN)	81.6%
			Maximum likelihood classification (MLC)	86.6%
Khan et al. [26]	Sundarbans	Landsat 5 TM, Landsat 7 ETM, and Landsat 8 OLI/30 m	MLC	62% in 2011 69% in 2021
Hao et al. [27]	Zhanjiang	Sentinel-2/10 m	Sem-dense connections by convolutional neural network	90.96%
de Souza Moreno et al. [28]	Cananéia-Iguape	Sentinel-1/5 m	U-Net with the Efficient-net-B7 backbone	85.77%
Our model	Zhanjiang, Taishan, and Maoming	GF-1, GF-6, ZY-3/2 m; GF-2/0.8 m	Attention U ² -Net	92.0%

A potential limitation of the attention U²-Net model is that it was developed based on satellite data acquired in three cities of Guangdong Province. Is the model applicable to the other regions? This has not been verified yet. This will be completed in the near future after more high-resolution satellite data are collected

4.2. Spatiotemporal Evolution of Mangroves in Shuidong Bay—A Case Study

Here we applied the attention U²-Net model to map the mangroves in Shuidong Bay as an example, which is a coastal area in Maoming City, Guangdong Province, China. We used 2 m resolution satellite images from 2015 to 2018 to analyze the spatial distribution and temporal evolution of mangroves in this area. The mangrove maps obtained from the model are shown in Figure 7, where the mangroves are marked in red and yellow. It can be seen that the mangroves are mainly distributed along the coastline of Shuidong Bay, and some of them are located in the estuaries of rivers. By using high-resolution satellite images, we can identify a large number of small mangrove patches that may be overlooked by other methods. These small patches are important for maintaining the biodiversity and ecosystem functions of mangroves. Figure 8 also shows the changes in the mangrove area over the four years. We can see that the mangrove forest expanded steadily from 2015 to 2018, with an average growth rate of over 10 hm² per year. The total area of mangroves increased by 17% in four years, reaching approximately 270 hm² in 2018. This indicates that the mangrove protection and management policy implemented by the local government in Maoming is effective, and that the mangrove restoration and conservation efforts have achieved positive results. The attention U²-Net model can provide useful information for monitoring and evaluating the status and trends of mangroves in Shuidong Bay, and it can also be applied to other regions with similar environmental conditions. This proves the important application value of this model for the long-term dynamic monitoring of mangroves. The research results are expected to provide useful feedback

information for government administrators, scientists, and other stakeholders related to mangrove dynamics.

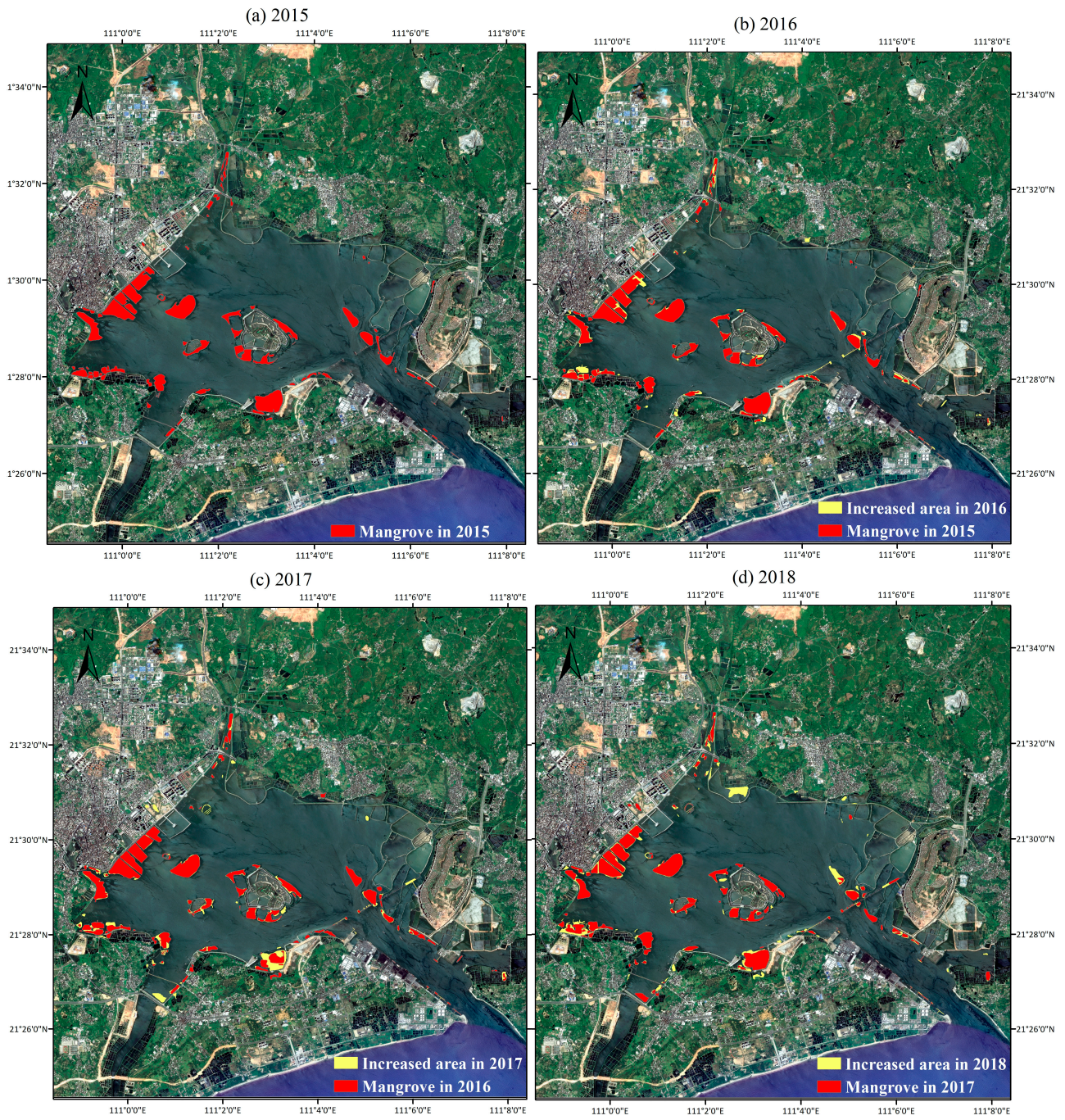


Figure 7. Distribution of mangroves in Shuidong Bay from 2015 to 2018.

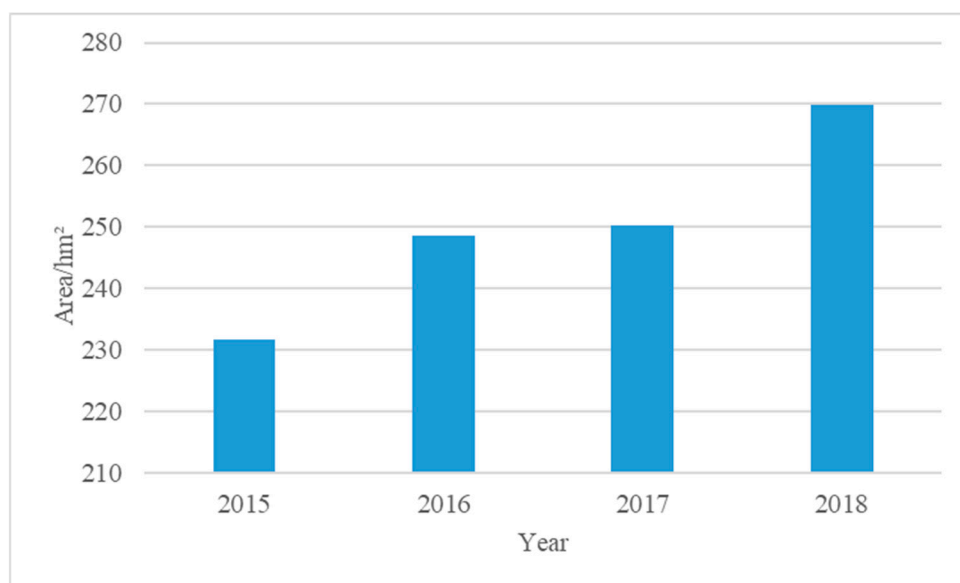


Figure 8. The area of mangroves from 2015 to 2018 in Maoming Shuidong Bay.

5. Conclusions

The main objective of this study is to realize automatic mangrove mapping from high-resolution images acquired by Chinese GF and ZY series satellites using a deep-learning method, i.e., the attention U²-Net model. The model can extract detailed features and boundaries of mangroves in coastal areas of Guangdong Province, China, and can also focus on the regions of interest and ignore the irrelevant regions by using an attention gate. The comparison with other machine-learning or deep-learning models (RF, U-Net, and U²-Net models) shows that our model generates the highest overall accuracy, precision, and F1 score values (96.5%, 92.0%, and 91.5%, respectively). By using high-resolution satellite images, we can obtain multi-scale information about mangroves, such as their location, area, shape, and density. Based on the mangrove maps generated by the model from high-resolution GF images, we found that the area of mangroves has steadily increased from 2015 to 2018 under the influence of China's mangrove planting policy, which aims to restore and conserve mangroves in coastal areas. The total area of mangroves has increased by 17% in four years, reaching approximately 270 hm² in 2018.

The combination of high-resolution satellite images and deep learning models helps to generate fine-scale mangrove maps, which can effectively support local authorities in mangrove planning and management. The fine-scale mangrove maps can provide useful information for assessing the status and trends of mangroves, evaluating the effectiveness of mangrove restoration and conservation efforts, and designing appropriate strategies and policies for the sustainable management of mangroves. Currently, our study is limited by the amount of collected field survey data, which are essential for training and validating the attention U²-Net model. The mangrove data were mainly collected in Guangdong coastal areas, where we established and evaluated our model. Therefore, we cannot assess the applicability and generalization ability of our model in other regions with different environmental conditions. However, with the increase of in situ measurements in the near future, we expect to improve our model and test its performance in other regions with similar or different types of mangroves.

Author Contributions: Conceptualization, X.L. and Q.X.; methodology, X.L., Y.C. and Q.X. and X.Y.; software, Y.C. and Y.W.; validation, Y.W.; formal analysis, Y.W.; investigation, J.K. and Y.C.; resources, J.K.; writing—original draft preparation, Y.W.; writing—review and editing, X.L., Q.X., Y.C., X.Y. and J.K., visualization, J.K.; supervision, Q.X., Y.C. and X.Y.; project administration, X.L. All authors have read and agreed to the published version of the manuscript.

Funding: This research was funded by the 1. 2022 Research Program of Sanya Yazhou Bay Science and Technology City: No. SKJC-2022-01-001; 2. National Natural Science Foundation of China: T2261149752; 3. National Natural Science Foundation of China: 41976163.

Informed Consent Statement: Not applicable.

Data Availability Statement: Not applicable.

Acknowledgments: The authors would like to thank the China Center for Resources Satellite Data and Application for providing Chinese GF-1, GF-2, GF-6, and ZY-3 satellite data products. The authors thank the U.S. Geological Survey for providing DEM data. Thanks for Dr Miao Chen's suggestions and assistance on algorithms and data processing during the revision process.

Conflicts of Interest: The authors declare no conflict of interest.

References

1. Yang, G.; Huang, K.; Sun, W.; Meng, X.; Mao, D.; Ge, Y. Enhanced mangrove vegetation index based on hyperspectral images for mapping mangrove. *ISPRS J. Photogramm. Remote Sens.* **2022**, *189*, 236–254. [CrossRef]
2. Jia, M.; Wang, Z.; Zhang, Y.; Mao, D.; Wang, C. Monitoring loss and recovery of mangrove forests during 42 years: The achievements of mangrove conservation in China. *Int. J. Appl. Earth Obs. Geoinf.* **2018**, *73*, 535–545. [CrossRef]
3. Hu, T.; Zhang, Y.; Su, Y.; Zheng, Y.; Lin, G.; Guo, Q. Mapping the global mangrove forest aboveground biomass using multisource remote sensing data. *Remote Sens.* **2020**, *12*, 1690. [CrossRef]
4. Aschbacher, J.; Ofren, R.; Delsol, J.P.; Suselo, T.B.; Vibulsresth, S.; Charrupat, T. An integrated comparative approach to mangrove vegetation mapping using advanced remote sensing and GIS technologies: Preliminary results. *Hydrobiologia* **1995**, *295*, 285–294. [CrossRef]
5. Thakur, S.; Mondal, I.; Ghosh, P.; Das, P.; De, T. A review of the application of multispectral remote sensing in the study of mangrove ecosystems with special emphasis on image processing techniques. *Spat. Inf. Res.* **2020**, *28*, 39–51. [CrossRef]
6. Kanniah, K.D.; Wai, N.S.; Shin, A.; Rasib, A.W. Per-pixel and sub-pixel classifications of high-resolution satellite data for mangrove species mapping. *Appl. GIS* **2007**, *3*, 1–22.
7. Wang, D.; Wan, B.; Qiu, P.; Su, Y.; Guo, Q.; Wu, X. Artificial mangrove species mapping using pléiades-1: An evaluation of pixel-based and object-based classifications with selected machine learning algorithms. *Remote Sens.* **2018**, *10*, 294. [CrossRef]
8. Pham, T.D.; Bui, D.T.; Yoshino, K.; Le, N.N. Optimized rule-based logistic model tree algorithm for mapping mangrove species using ALOS PALSAR imagery and GIS in the tropical region. *Environ. Earth Sci.* **2018**, *77*, 159. [CrossRef]
9. Kamal, M.; Jamaluddin, I.; Parella, A.; Farda, N.M. Comparison of Google Earth Engine (GEE)-based machine learning classifiers for mangrove mapping. In Proceedings of the 40th Asian Conference Remote Sensing, ACRS, Daejeon, Republic of Korea, 14–18 October 2019; pp. 1–8.
10. Nagarajan, P.; Rajendran, L.; Pillai, N.D.; Lakshmanan, G. Comparison of machine learning algorithms for mangrove species identification in Malad creek, Mumbai using WorldView-2 and Google Earth images. *J. Coast. Conserv.* **2022**, *26*, 44. [CrossRef]
11. Zhang, S.; Xu, Q.; Wang, H.; Kang, Y.; Li, X. Automatic waterline extraction and topographic mapping of tidal flats from SAR images based on deep learning. *Geophys. Res. Lett.* **2022**, *49*, e2021GL096007. [CrossRef]
12. Liu, B.; Li, X.; Zheng, G. Coastal inundation mapping from bitemporal and dual-polarization SAR imagery based on deep convolutional neural networks. *J. Geophys. Res. Ocean.* **2019**, *124*, 9101–9113. [CrossRef]
13. Xie, H.; Xu, Q.; Cheng, Y.; Yin, X.; Jia, Y. Reconstruction of subsurface temperature field in the south China Sea from satellite observations based on an attention U-net model. *IEEE Trans. Geosci. Remote Sens.* **2022**, *60*, 4209319. [CrossRef]
14. Iovan, C.; Kulbicki, M.; Mermet, E. Deep convolutional neural network for mangrove mapping. In Proceedings of the IGARSS 2020—2020 IEEE International Geoscience and Remote Sensing Symposium, Waikoloa, HI, USA, 26 September–2 October 2020; pp. 1969–1972.
15. Huang, Y.Q.; Liu, Q.; Zhao, J.H.; Huang, W.S.; Sun, Z.X.; Qiao, X. Research on mangrove drone monitoring based on convolutional neural network. *China Agric. Mach. Chem. News* **2020**, *41*, 141–146, 189.
16. Guo, Y.; Liao, J.; Shen, G. Mapping large-scale mangroves along the maritime silk road from 1990 to 2015 using a novel deep learning model and landsat data. *Remote Sens.* **2021**, *13*, 245. [CrossRef]
17. Hu, L.; Xu, N.; Liang, J.; Li, Z.; Chen, L.; Zhao, F. Advancing the mapping of mangrove forests at national-scale using Sentinel-1 and Sentinel-2 time-series data with Google Earth Engine: A case study in China. *Remote Sens.* **2020**, *12*, 3120. [CrossRef]
18. Zhang, Y.; Xiao, F.; Mei, H.; Li, Y.; Liu, C.; Qiu, X. Comprehensive analysis of climate-related comfort in southern China: Climatology, trend, and interannual variations. *Urban Clim.* **2022**, *46*, 101349. [CrossRef]
19. PIE-Ortho Software. Available online: <http://www.piesat.cn/website/cn/pages/product/software/pie-ortho.html> (accessed on 14 March 2020).
20. Cooley, T.; Anderson, G.P.; Felde, G.W.; Hoke, M.L.; Ratkowski, A.J.; Chetwynd, J.H.; Gardner, J.A.; Adler-Golden, S.M.; Matthew, M.W.; Berk, A. FLAASH, a MODTRAN4-based atmospheric correction algorithm, its application and validation. In Proceedings of the IEEE International Geoscience and Remote Sensing Symposium, Toronto, ON, Canada, 24–28 June 2002; pp. 1414–1418.
21. Zhang, Y. System and Method for Image Fusion. U.S. Patent No. 7340099, 4 March 2008.

22. Qin, X.; Zhang, Z.; Huang, C.; Dehghan, M.; Zaiane, O.R.; Jagersand, M. U²-Net: Going deeper with nested U-structure for salient object detection. *Pattern Recognit.* **2020**, *106*, 107404. [[CrossRef](#)]
23. Oktay, O.; Schlemper, J.; Folgoc, L.L.; Lee, M.; Heinrich, M.; Misawa, K.; Mori, K.; McDonagh, S.; Hammerla, N.Y.; Kainz, B. Attention u-net: Learning where to look for the pancreas. *arXiv* **2018**, arXiv:1804.03999.
24. Smith, L.N. Cyclical learning rates for training neural networks. In Proceedings of the 2017 IEEE Winter Conference on Applications of Computer Vision (WACV), Santa Rosa, CA, USA, 24–31 March 2017; pp. 464–472.
25. Wang, L.; Silván-Cárdenas, J.L.; Sousa, W.P. Neural network classification of mangrove species from multi-seasonal Ikonos imagery. *Photogramm. Eng. Remote Sens.* **2008**, *74*, 921–927. [[CrossRef](#)]
26. Khan, A.R.; Khan, A.; Masud, S.; Rahman, R.M. Analyzing the Land Cover Change and Degradation in Sundarbans Mangrove Forest Using Machine Learning and Remote Sensing Technique. In Proceedings of the Advances in Computational Intelligence: 16th International Work-Conference on Artificial Neural Networks, IWANN 2021, Virtual Event, 16–18 June 2021; Proceedings, Part II 16, 2021. pp. 429–438.
27. Hao, C.; Sang, H.Y.; Zhai, L.; Zhu, H. A mangrove extraction method combined with sem-dense connections by convolutional neural network. *Sci. Surv. Mapp.* **2022**, *47*, 146–152.
28. De Souza Moreno, G.M.; de Carvalho Júnior, O.A.; de Carvalho, O.L.F.; Andrade, T.C. Deep semantic segmentation of mangroves in Brazil combining spatial, temporal, and polarization data from Sentinel-1 time series. *Ocean Coast. Manag.* **2023**, *231*, 106381. [[CrossRef](#)]

Disclaimer/Publisher’s Note: The statements, opinions and data contained in all publications are solely those of the individual author(s) and contributor(s) and not of MDPI and/or the editor(s). MDPI and/or the editor(s) disclaim responsibility for any injury to people or property resulting from any ideas, methods, instructions or products referred to in the content.